Author(s): Hinkkanen, M.

Title: Analysis and Design of Full-Order Flux Observers for Sensorless Induction Motors

Year: 2004

Version: Post print

Please cite the original version:

Hinkkanen, M. 2004. Analysis and Design of Full-Order Flux Observers for Sensorless Induction Motors. IEEE Transactions on Industrial Electronics. Volume 51, Issue 5. 1033-1040. ISSN 0278-0046 (printed). DOI: 10.1109/tie.2004.834964.

Analysis and Design of Full-Order Flux Observers for Sensorless Induction Motors

Marko Hinkkanen

***Abstract*—This paper deals with the flux estimation for sensorless induction motor drives. The linearized model of the speed-adaptive full-order flux observer is applied to help choosing the observer gain and the speed-adaptation gains. It is shown that the linearized model reveals potential instability problems that are difficult to find by other means. An observer gain and a method to vary the speed-adaptation gains in the field-weakening region are proposed. Experimental results show stable operation in a very wide speed range.**

***Index Terms*—Flux estimation, full-order adaptive observer, induction motor drives, speed sensorless.**

I. Introduction

Speed-sensorless induction motor drives have developed significantly during the last few years. Speed-adaptive full-order flux observers [1], [2] are promising flux estimators for induction motor drives. The speed-adaptation mechanism seems to imply tolerance of measurement noise, and the flexible observer structure makes it possible to use same analysis tools and experimental algorithms for different observer designs.

The speed-adaptive observer consists of a state-variable observer augmented with a speed-adaptation loop. The observer gain and the speed-adaptation law determine the properties of the observer. The observer gain is often chosen to be zero [1], [3]–[5]. If a nonzero observer gain is used, the gain is usually selected by ignoring the effect of the speed-adaptation loop and using pole placement [2], [6], [7].

However, the speed-adaptive observer is a nonlinear system, even if a constant rotor speed is assumed. The speed-adaptation loop affects considerably the dynamics of the observer and may cause unstable regions. Instability problems encountered in the regenerating mode at low speeds are well known [3], [5], [8]–[10]. Speed-sensorless reduced-order observers may also have similar problems in the regenerating mode as shown in [11]. There is also a risk of instability at higher speeds if the observer gain is zero or poorly selected. Furthermore, inappropriate gains may unnecessarily lower the bandwidth of the speed estimation in the field-weakening region. Therefore, the speed estimation should be incorporated into the analysis. A straightforward way to do this is to linearize the observer for analysis purposes.

Even though some authors have taken the speed-adaptation loop into account in the analysis of full-order observers [3], [8], [9], [12], the application of linearized models to the gain selection for a wide speed range operation has not been considered. However, linearized models have been successfully applied to reduced-order observers in [13].

This paper applies the linearized model of the observer to help selecting the observer gain and the speed-adaptation gains. The induction motor model and the speed-adaptive flux observer are first defined. Then, the linearized model of the speed-adaptive observer is introduced. Based on the model, an observer gain and a method to vary the speed-adaptation gains in the field-weakening region are proposed. Finally, a control system based on the rotor flux orientation is described and experimental results are presented.

The author is with the Power Electronics Laboratory, Helsinki University of Technology, FIN-02015 HUT, Espoo, Finland (email: marko.hinkkanen@hut.fi).

II. Induction Motor Model

The parameters of the inverse-Γ-equivalent circuit [14] of an induction motor are the stator resistance R_s, the rotor resistance R_R, the stator transient inductance L'_s, and the magnetizing inductance L_M. The electrical angular speed of the rotor is denoted by ω_m, the angular speed of the reference frame ω_k, the stator current space vector $\underline{i}_s$, and the stator voltage $\underline{u}_s$. When the stator flux $\underline{\psi}_s$ and the rotor flux $\underline{\psi}_R$ are chosen as state variables, the state-space representation of the induction motor becomes

$$\dot{\underline{\mathbf{x}}} = \underbrace{\begin{bmatrix} -\frac{1}{\tau'_s} - j\omega_k & \frac{1}{\tau'_s} \\ \frac{1-\sigma}{\tau'_r} & -\frac{1}{\tau'_r} - j\left(\omega_k - \omega_m\right) \end{bmatrix}}_{\mathbf{A}} \underline{\mathbf{x}} + \underbrace{\begin{bmatrix} 1 \\ 0 \end{bmatrix}}_{\mathbf{B}} \underline{u}_s \tag{1a}$$

$$\underline{i}_s = \underbrace{\begin{bmatrix} \frac{1}{L'_s} & -\frac{1}{L'_s} \end{bmatrix}}_{\mathbf{C}} \underline{\mathbf{x}} \tag{1b}$$

where the state vector is $\underline{\mathbf{x}} = [\underline{\psi}_s \quad \underline{\psi}_R]^T$, and the parameters are $\sigma = L'_s/(L_M + L'_s)$, $\tau'_s = L'_s/R_s$, and $\tau'_r = \sigma L_M/R_R$. The electromagnetic torque is

$$T_e = \frac{3}{2} p \operatorname{Im}\left\{\underline{i}_s \underline{\psi}^*_R\right\} = \frac{3}{2} p \frac{1}{L'_s} \operatorname{Im}\left\{\underline{\psi}_s \underline{\psi}^*_R\right\} \tag{2}$$

where p is the number of pole pairs and the complex conjugates are marked by the symbol *.

III. Speed-Adaptive Full-Order Flux Observer

Choosing the stator and rotor fluxes as state variables is preferred since no inductance derivatives are needed and the modelling of magnetic saturation becomes simpler. In addition, the observer could be used with stator flux orientation control or direct torque control [7] as well as with rotor flux orientation

control. Consequently, the full-order flux observer is defined by

$$\dot{\hat{\underline{\mathbf{x}}}} = \hat{\underline{\mathbf{A}}}\,\hat{\underline{\mathbf{x}}} + \mathbf{B}\underline{u}_s + \underline{\mathbf{L}}\big(\underline{i}_s - \hat{\underline{i}}_s\big) \tag{3a}$$

$$\hat{\underline{i}}_s = \mathbf{C}\hat{\underline{\mathbf{x}}} \tag{3b}$$

where the observer state vector is $\hat{\underline{\mathbf{x}}} = [\hat{\underline{\psi}}_s \quad \hat{\underline{\psi}}_R]^T$ and the estimates are marked by the symbol $\hat{}$. The matrix $\hat{\underline{\mathbf{A}}}$ and the observer gain $\underline{\mathbf{L}}$ are given by

$$\hat{\underline{\mathbf{A}}} = \begin{bmatrix} -\frac{1}{\tau'_s} - j\omega_k & \frac{1}{\tau'_s} \\ \frac{1-\sigma}{\tau'_r} & -\frac{1}{\tau'_r} - j(\omega_k - \hat{\omega}_m) \end{bmatrix}, \quad \underline{\mathbf{L}} = \begin{bmatrix} \underline{l}_s \\ \underline{l}_r \end{bmatrix} \tag{3c}$$

If the conventional state variables are preferred, a transformation of the observer gains given in Appendix A can be used.

The rotor speed is estimated using the adaptation mechanism [1], [2]

$$\hat{\omega}_m = -\gamma_p\,\varepsilon - \gamma_i \int \varepsilon\, dt \tag{4a}$$

where γ_p and γ_i are positive adaptation gains and

$$\varepsilon = \mathrm{Im}\left\{\big(\underline{i}_s - \hat{\underline{i}}_s\big)\hat{\underline{\psi}}_R^*\right\} \tag{4b}$$

is an error term. According (4b), the speed estimation is based on the component of the current estimation error which is perpendicular to the estimated rotor flux.

A. Stability

The speed-adaptation law (4) was originally derived using the Lyapunov stability theory [1] or the Popov hyperstability theory [2]. However, the stability of the adaptation law is not guaranteed. The derivation in [1] neglects a term including the actual rotor flux (which is not measurable) as shown in [5]. The positive-realness condition is not satisfied in [2] as shown in [8]. A modified speed-adaptation law based on the current estimation error perpendicular to the estimated stator flux was proposed in [7], [12]. The behavior and the unstable regions of the modified adaptation law are virtually the same as those of (4).

An unstable region encountered at low speeds with regenerative loads is well known. An observer gain design reducing the region was considered in [8]. An observer gain stabilizing the regenerating mode at low speeds was proposed in [9]. An alternative approach to stabilize the regenerating mode is to modify the speed-adaptation law [3], [10]. As shown in Section V, another instability may occur in the field-weakening region when typical observer design is used.

It is desired to have a wide speed and torque range with good dynamic properties. The approach used in this paper is to design the observer gain especially for nominal and high-speed operation whereas the problems at low speeds in the regenerating mode can be handled by modifying the speed-adaptation law as shown in [10].

B. Relationship to Conventional Model-Reference Adaptive System (MRAS)

It is interesting to consider the relationship between the speed-adaptive observer (3) and (4), and the conventional MRAS[1] flux estimator consisting of the voltage model and the current model [15]. By choosing the observer gain

$$\underline{\mathbf{L}} = \begin{bmatrix} -R_s \\ R_R \end{bmatrix} \tag{5}$$

the voltage model and the current model are obtained from (3). The error term (4b) of the adaptation law can be written as

$$\varepsilon = -\frac{1}{L'_s}\,\mathrm{Im}\left\{\big(\hat{\underline{\psi}}_s - L'_s\underline{i}_s\big)\hat{\underline{\psi}}_R^*\right\} \tag{6}$$

based on (3b). Comparison of (6) and the speed-adaptation law in [15] shows that the adaptation laws are identical; only the adaptation gains are scaled by L'_s. The factor $\hat{\underline{\psi}}_s - L'_s\underline{i}_s$ is the output of the voltage model whereas $\hat{\underline{\psi}}_R$ is the output of the current model. Hence the conventional MRAS is a special case of the more general speed-adaptive flux observer. Regardless of operating point, the conventional MRAS is only marginally stable (poles on the imaginary axis).

IV. Linearized Model

The nonlinear and complicated dynamics of the speed-adaptive observer can be studied via small-signal linearization. The key factor in the linearization is to use a synchronous reference frame in order to obtain a steady-state operating point. In the following, the dynamics of both the motor and the observer are taken into account. Even though the stator dynamics are included in the model, the linearized model is independent of the stator voltage and, consequently, of the current controller. Accurate motor parameter estimates are assumed in the analysis.

A. Estimation Error

The nonlinear dynamics of the estimation error $\underline{\mathbf{e}} = \underline{\mathbf{x}} - \hat{\underline{\mathbf{x}}}$ of the state vector can be written based on (1) and (3)

$$\begin{aligned} \dot{\underline{\mathbf{e}}} &= \big(\underline{\mathbf{A}} - \underline{\mathbf{L}}\mathbf{C}\big)\,\underline{\mathbf{x}} - \big(\hat{\underline{\mathbf{A}}} - \underline{\mathbf{L}}\mathbf{C}\big)\hat{\underline{\mathbf{x}}} \\ &= \big(\underline{\mathbf{A}} - \underline{\mathbf{L}}\mathbf{C}\big)\,\underline{\mathbf{e}} + \begin{bmatrix} 0 \\ j\hat{\underline{\psi}}_R \end{bmatrix}(\omega_m - \hat{\omega}_m) \end{aligned} \tag{7}$$

In the estimated rotor flux reference frame, the linearized model of (7) becomes (see Appendix B)

$$\dot{\underline{\mathbf{e}}} = \big(\underline{\mathbf{A}}_0 - \underline{\mathbf{L}}_0\mathbf{C}\big)\,\underline{\mathbf{e}} + \begin{bmatrix} 0 \\ j\psi_{R0} \end{bmatrix}(\omega_m - \hat{\omega}_m) \tag{8a}$$

Here, the operating-point quantities are marked by the subscript 0, and the matrices are

$$\underline{\mathbf{A}}_0 = \begin{bmatrix} -\frac{1}{\tau'_s} - j\omega_{s0} & \frac{1}{\tau'_s} \\ \frac{1-\sigma}{\tau'_r} & -\frac{1}{\tau'_r} - j\omega_{r0} \end{bmatrix}, \quad \underline{\mathbf{L}}_0 = \begin{bmatrix} \underline{l}_{s0} \\ \underline{l}_{r0} \end{bmatrix} \tag{8b}$$

where the stator angular frequency is ω_{s0} and the slip angular frequency is $\omega_{r0} = \omega_{s0} - \omega_{m0}$.

The transfer function from the estimation error of the speed $\omega_m - \hat{\omega}_m$ to the estimation error of the current $\underline{i}_s - \hat{\underline{i}}_s$ is

$$\begin{aligned} \underline{G}(s) &= \mathbf{C}\left(s\mathbf{I} - \underline{\mathbf{A}}_0 + \underline{\mathbf{L}}_0\mathbf{C}\right)^{-1}\begin{bmatrix} 0 \\ j\psi_{R0} \end{bmatrix} \\ &= -\frac{j\psi_{R0}}{L'_s}\,\frac{s + j\omega_{s0}}{A(s) + jB(s)} \end{aligned} \tag{9a}$$

[1]Even though the speed-adaptive observer can also be considered as an MRAS, the term conventional MRAS is used here to refer only to the flux estimator in [15].

where $\mathbf{I} = \left[\begin{smallmatrix}1 & 0\\ 0 & 1\end{smallmatrix}\right]$ is the identity matrix. The polynomials in (9a) are defined as

$$A(s) = s^2 + s\left(\frac{1}{\tau_s'} + \frac{1}{\tau_r'} + \frac{l_{sd0} - l_{rd0}}{L_s'}\right) - \omega_{s0}\omega_{r0} + \frac{\sigma}{\tau_s'\tau_r'} + \frac{\omega_{s0}l_{rq0} - \omega_{r0}l_{sq0}}{L_s'} + \frac{\sigma l_{sd0}}{\tau_r' L_s'} \tag{9b}$$

$$B(s) = s\left(\omega_{s0} + \omega_{r0} + \frac{l_{sq0} - l_{rq0}}{L_s'}\right) + \frac{\omega_{s0}\tau_s' + \omega_{r0}\tau_r'}{\tau_s'\tau_r'} + \frac{\omega_{r0}l_{sd0} - \omega_{s0}l_{rd0}}{L_s'} + \frac{\sigma l_{sq0}}{\tau_r' L_s'} \tag{9c}$$

where the entries of the observer gain are divided into real and imaginary components: $\underline{l}_{s0} = l_{sd0} + jl_{sq0}$ and $\underline{l}_{r0} = l_{rd0} + jl_{rq0}$. Since the observer gain is allowed to be a function of the estimated rotor speed, the subscript 0 is used in the equations. It is to be noted that $\underline{G}(s)$ is independent of the speed-adaptation law.

B. Speed-Adaptation Law

In the estimated rotor flux reference frame, the rotor flux estimate is $\underline{\hat{\psi}}_R = \hat{\psi}_R + j0$ and the adaptation law (4) reduces to

$$\hat{\omega}_m = -\gamma_p(i_{sq} - \hat{i}_{sq})\hat{\psi}_R - \gamma_i \int (i_{sq} - \hat{i}_{sq})\hat{\psi}_R \, dt \tag{10}$$

The linearized transfer function from the current error $i_{sq} - \hat{i}_{sq}$ to the speed estimate $\hat{\omega}_m$ is

$$K(s) = -\left(\gamma_{p0} + \frac{\gamma_{i0}}{s}\right)\psi_{R0} \tag{11}$$

where the gains can be functions of the speed estimate.

Based on (10), only the imaginary component $i_{sq} - \hat{i}_{sq}$ of the estimation error of the current is of interest. Thus the imaginary component of $\underline{G}(s)$ is used,

$$G_q(s) = \mathrm{Im}\{\underline{G}(s)\} = -\frac{\psi_{R0}}{L_s'}\frac{sA(s) + \omega_{s0}B(s)}{A^2(s) + B^2(s)} \tag{12}$$

Using (11) and (12), the closed-loop system shown in Fig. 1 is formed. The closed-loop transfer function

$$G_{cl}(s) = \frac{\hat{\omega}_m(s)}{\omega_m(s)} = \frac{G_q(s)K(s)}{1 + G_q(s)K(s)} \tag{13}$$

corresponding to any operating point can be easily calculated using suitable computer software (e.g., MATLAB Control System Toolbox).

When calculating the transfer functions, the magnitude of the rotor flux ψ_{R0} is lowered in the field-weakening region corresponding to the applied field-weakening scheme. In this paper, the conventional $1/\hat{\omega}_m$-method is used and the steady-state flux becomes

$$\psi_{R0} = \begin{cases} \psi_\gamma, & \text{if } |\omega_{m0}| \le \omega_\gamma \\ \psi_\gamma \frac{\omega_\gamma}{|\omega_{m0}|}, & \text{if } |\omega_{m0}| > \omega_\gamma \end{cases} \tag{14}$$

where the field-weakening point is ω_γ and the flux in the base-speed region is ψ_γ.

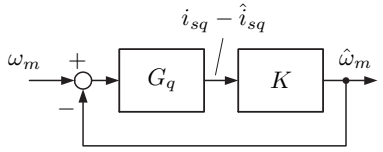

Fig. 1. Block diagram presenting linearized model of speed-adaptive full-order flux observer.

V. Gain Selection

The gain selection can be studied using the linearized model in Fig. 1. A variety of analysis methods of linear systems, e.g., pole-zero plots and frequency responses, can be exploited.

Pole locations of $G_{cl}(s)$ can reveal improper selection of the gains. A system is stable if the poles are located in the left half of the complex plane. To obtain good transient behavior (i.e., fastness, good damping, low sensitivity to noise), additional constraints of the pole locations are needed.

Poorly placed poles (e.g., imaginary parts of poles much larger than the corresponding rotor speed ω_{m0}, or real parts far away in the left half-plane or too close to the imaginary axis) may cause an oscillating, noisy, or too slow behavior of the system. When the speed-adaptation gains γ_{p0} and γ_{i0} approach zero, the poles approach the poles of the speed-sensored case (the eigenvalues of (3) when $\hat{\omega}_m = \omega_m$). In addition, there is a pole in the origin. When the adaptation gains increase, the poles begin to deviate from the poles of the speed-sensored case and from the origin.

There are also zeros of $G_{cl}(s)$ affecting the system. Even though the poles determine the stability of the system, the location of zeros may give useful information of the transient behavior of the system. Furthermore, the bandwidth of the speed estimation, which limits the bandwidth of the speed controller, can be obtained from the frequency response $G_{cl}(j\omega)$.

In the following, a typical way to select the gains is first described. It is shown that the zero observer gain may lead to an unstable operation region at higher speeds. Then, gain scheduling giving well-behaving dynamics in a very wide speed range is proposed.

A. Typical Gains

The observer gain $\underline{\mathbf{L}}$ is usually chosen to be zero. Since the current estimation error acts as a feedback through the speed estimation, zero observer gain does not imply an open-loop simulation. The speed-adaptation gains γ_p and γ_i are normally constants tuned in the base-speed region. The gains can be selected experimentally: first $\gamma_p = 0$ is selected and the maximum value of γ_i is found, then γ_p is maximized with the fixed γ_i.

An example of variations of the poles and zeros of $G_{cl}(s)$, obtained using the zero observer gain and constant speed-adaptation gains, is shown in Fig. 2. The parameters of a 2.2-kW four-pole induction motor given in Table I were used. The base value of the angular frequency is $2\pi \cdot 50$ s^{-1}. At the rotor speed of 1.4 p.u., the dominant complex-conjugate pair of the poles is close to the imaginary axis. Poor damping due to this pole location may cause problems in practice. If γ_p close to zero were chosen, a part of the locus would even be

TABLE I
PARAMETERS OF 2.2-KW 4-POLE 400-V 50-HZ MOTOR AND LOAD

Stator resistance R_s	3.67 Ω
Rotor resistance R_R	2.10 Ω
Magnetizing inductance L_M	0.224 H
Stator transient inductance L'_s	0.0209 H
Rated speed	1 430 r/min
Rated current	5.0 A
Rated torque	14.6 Nm
Total moment of inertia	0.0155 kgm^2
Viscous friction coefficient	0.0025 Nm·s

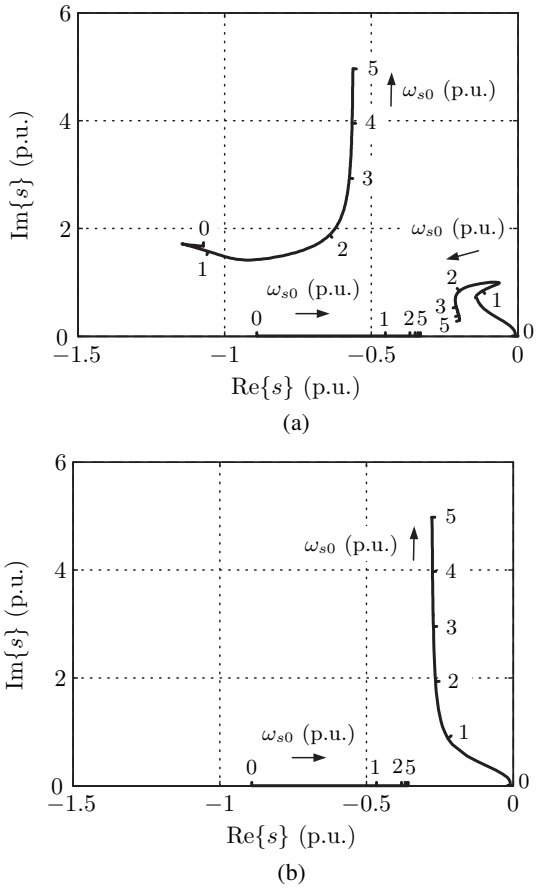

Fig. 2. Variation of (a) poles and (b) zeros of $G_{cl}(s)$, when typical gains are used. Stator frequency is $\omega_{s0} = 0...5$ p.u. and slip frequency ω_{r0} is rated. Observer parameters are $\gamma_p = 10$ (Nm·s)$^{-1}$, $\gamma_i = 10\,000$ (Nm·s^2)$^{-1}$, and $\underline{\mathbf{L}} = [0 \quad 0]^T$. Due to symmetry, only upper half-plane is shown.

in the right half-plane. If the sign of the slip frequency were changed (corresponding to the regenerating mode), one real pole would be in the right half-plane at low speeds.

The dashed line in Fig. 3 depicts an example of the frequency response $G_{cl}(j\omega)$, an operating point corresponding to the stator frequency 3 p.u. and the rated slip. Based on Fig. 3, the bandwidth of the speed estimation is 0.81 p.u. Furthermore, there is a resonant peak having the gain of 1.45. By examining the frequency response at different operating points, it can be noticed that the bandwidth of the speed estimation decreases significantly at high speeds in the field-weakening region.

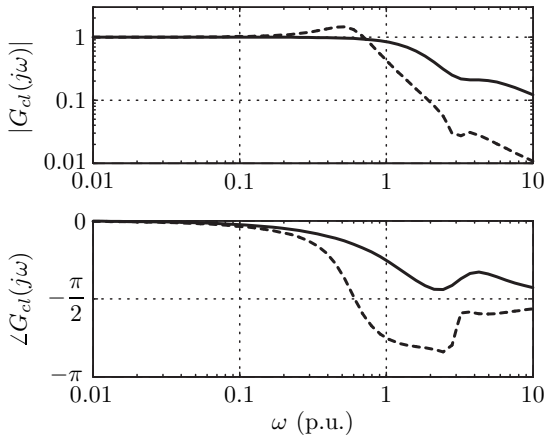

Fig. 3. Frequency response $G_{cl}(j\omega)$. Stator frequency is $\omega_{s0} = 3$ p.u. and slip frequency ω_{r0} is rated. Dashed and solid line correspond to observer using typical gains and proposed gains, respectively.

B. Proposed Gains

1) Speed-Adaptation Gains: The field weakening reduces the loop gain $G_q(s)K(s)$, thus reducing the bandwidth of the speed estimation. The effect of the field weakening (14) can be compensated by selecting the gains

$$\gamma_p = \begin{cases} \gamma'_p, & \text{if } |\hat{\omega}_m| \le \omega_\gamma \\ \gamma'_p \frac{\hat{\omega}_m^2}{\omega_\gamma^2}, & \text{if } |\hat{\omega}_m| > \omega_\gamma \end{cases} \tag{15a}$$

$$\gamma_i = \begin{cases} \gamma'_i, & \text{if } |\hat{\omega}_m| \le \omega_\gamma \\ \gamma'_i \frac{\hat{\omega}_m^2}{\omega_\gamma^2}, & \text{if } |\hat{\omega}_m| > \omega_\gamma \end{cases} \tag{15b}$$

where γ'_p and γ'_i are the base-speed region values of the proportional and integral gains, respectively. In other field-weakening schemes, the compensation can be carried out in a similar manner. For different motor sizes, the suitable values of γ'_p and γ'_i are usually proportional to the corresponding values of L'_s/ψ_γ^2.

2) Observer Gain: Different observer gains can be easily studied using the linearized model of the observer. It was discovered that real-valued gains cannot give enough damping at high speeds. A simple complex-valued observer gain

$$\underline{\mathbf{L}} = \lambda \begin{bmatrix} 1 + j\,\mathrm{sign}(\hat{\omega}_m) \\ -1 + j\,\mathrm{sign}(\hat{\omega}_m) \end{bmatrix} \tag{16a}$$

was found satisfying, where

$$\lambda = \begin{cases} \lambda' \frac{|\hat{\omega}_m|}{\omega_\lambda}, & \text{if } |\hat{\omega}_m| < \omega_\lambda \\ \lambda', & \text{if } |\hat{\omega}_m| \ge \omega_\lambda \end{cases} \tag{16b}$$

The positive constants λ' and ω_λ can be selected based on the linearized model. The parameter λ' can be considered as an impedance, which may be helpful when choosing λ' for different motor sizes. The transformation in Appendix A can be used for comparing the proposed observer gain with gains designed previously for the conventional state variables. It is interesting to note that, at nominal and high speeds, the proposed gain (16) has similarities (e.g., the same signs of the real and imaginary components) with the gain proposed in [6].

An example of variations of poles and zeros of $G_{cl}(s)$, obtained using the proposed gains (15) and (16), is shown

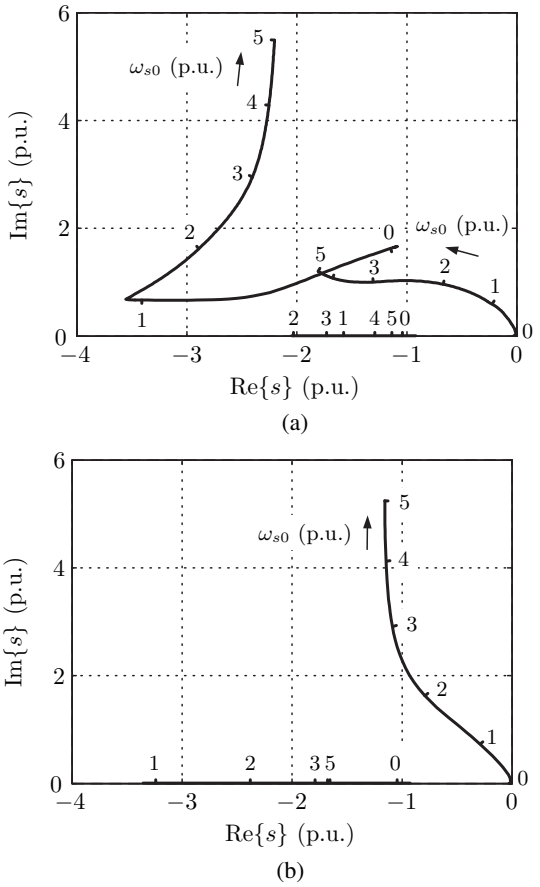

Fig. 4. Variation of (a) poles and (b) zeros of $G_{cl}(s)$, when proposed gains are used. Stator frequency is $\omega_{s0} = 0...5$ p.u. and slip frequency ω_{r0} is rated. Observer parameters are $\gamma_p' = 10$ (Nm·s)$^{-1}$, $\gamma_i' = 10\,000$ (Nm·s^2)$^{-1}$, $\lambda' = 10\ \Omega$, and $\omega_\lambda = 1$ p.u. Due to symmetry, only upper half-plane is shown.

in Fig. 4. It can be seen that the problem of poor damping encountered at higher speeds is removed. Furthermore, it can be shown that the unstable region in the regenerating mode at low speeds is slightly reduced as compared with the zero observer gain case. The unstable region could be reduced even more by modifying the observer gain or the speed-adaptation law in the low-speed region. A modified speed-adaptation law (compatible with the proposed gains) stabilizing the regenerating mode was proposed in [10].

The solid line in Fig. 3 shows an example of the frequency response $G_{cl}(j\omega)$. The bandwidth of the speed estimation is 1.33 p.u. and there is no resonant peak. By examining the frequency response at different operating points, it can be noticed that the bandwidth of the speed estimation at high speeds is increased as compared with the typical gains.

VI. Control System

The speed-adaptive observer was investigated experimentally using the setup shown in Fig. 5. The 2.2-kW induction motor (Table I) was fed by a frequency converter controlled by a dSpace DS1103 PPC/DSP board. The control system was based on the rotor flux orientation. The simplified overall block diagram of the system is shown in Fig. 6. The digital implementation of the observer proposed in [16] was used.[2] Unless otherwise noted, the parameters of the observer correspond to the parameters used in Fig. 4. The field-weakening point was $\omega_\gamma = 0.85$ p.u. and the flux in the base-speed region $\psi_\gamma = 0.9$ Wb.

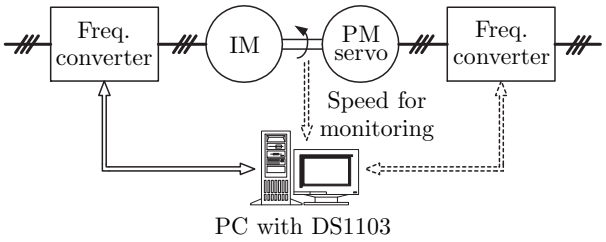

Fig. 5. Experimental setup. Permanent magnet (PM) servo motor was used as loading machine.

A PI-type synchronous-frame current controller including the decoupling of the back-emf voltages was used [18]. The bandwidth of the current controller was 8 p.u. The speed estimate used outside the observer was filtered using a first-order low-pass filter having the bandwidth of 0.8 p.u. The speed controller was a conventional PI-controller having the base-speed region bandwidth of 0.16 p.u. In the field-weakening region, the actual bandwidth of the speed controller was reduced proportionally to the flux, i.e., the gain from the reference torque $T_{e,\mathrm{ref}}$ to the q-component of the reference current $i_{sq,\mathrm{ref}}$ was kept constant, $2/(3p\psi_\gamma)$.

The flux controller was a PI-type controller including a feedforward term [19]. The bandwidth of the feedforward path was limited to 0.16 p.u. The bandwidth of the feedback loop was linearly increased from 0.016 p.u. to 0.16 p.u. corresponding to $\hat{\omega}_m$ changing from ω_γ to $2\omega_\gamma$. For speeds higher than $2\omega_\gamma$, the bandwidth was 0.16 p.u.

The sampling was synchronized to the modulation, and both the switching frequency and the sampling frequency were 5 kHz. The dc-link voltage was measured, and the reference voltage obtained from the current controller was used for the flux observer. A simple current feedforward compensation for dead times and power device voltage drops was applied [20].

VII. Experimental Results

The base values used in the following figures are: current $\sqrt{2} \cdot 5.0$ A and flux 1.0 Wb. Experimental results obtained using the typical gains corresponding to those used in Fig. 2 are shown in Fig. 7(a). The speed reference was stepped from zero to 1.4 p.u. at $t = 0.5$ s. A rated-load torque step was applied approximately at $t = 1.5$ s. It can be seen that the system becomes unstable after the load torque step. At slightly lower or higher speeds, similar problems were not encountered.

The instability is explained by the closed-loop poles shown in Fig. 2(a). At speed 1.4 p.u., the dominant complex-conjugate pair of the poles is close to the imaginary axis. Under the load torque, the actual slip frequency is larger than

[2]Computationally more efficient digital implementation given in [17] could also be used.

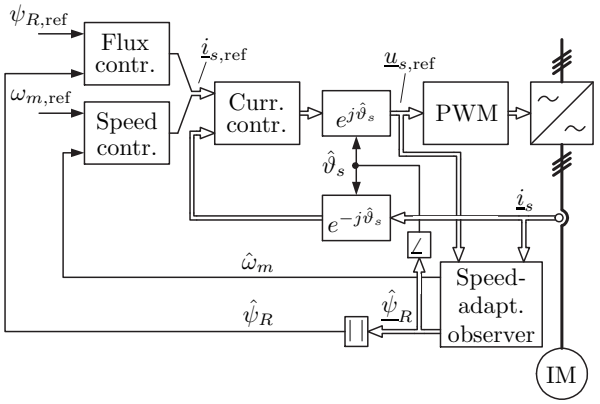

Fig. 6. Rotor flux oriented controller. Electrical variables shown on left-hand side of coordinate transformations are in estimated flux reference frame and variables on right-hand side are in stator reference frame.

the rated one since the drive is operating in the field-weakening region. In the pole plot, the larger slip frequency would shift the corresponding poles slightly more to the right. Even though the linearized model remains stable, the real system becomes unstable due to noise, poor damping of the observer dynamics, and high bandwidths of the controllers. The system remained stable when the bandwidths of the speed and flux controllers were significantly decreased.

Fig. 7(b) shows experimental results obtained using the proposed gains corresponding to those used in Fig. 4. As expected, the system behaves stably. The noise in the currents during the acceleration and under the load torque is caused by overmodulation. Under the load torque, all voltage available is used and thus the reference speed cannot be achieved.

High-speed operation is demonstrated in Fig. 8. The speed reference was stepped from zero to 5 p.u. at $t = 1$ s. No external load torque was applied.[3] The drive is operating in the overmodulation region even in the steady state due to high mechanical losses. Since the speed estimate is obtained through integration, the noise of the estimate is not a problem and thus operation at very high speeds is possible.

Experimental results showing zero-speed operation during the rated-load torque step are shown in Fig. 9. In this experiment, the bandwidth of the speed controller was 0.32 p.u. The speed reference was set to zero. The rated-load torque step was applied at $t = 4$ s, and the load torque was removed at $t = 12$ s. It can be seen that both the flux and the speed are correctly observed. After removing the load, the flux is still properly estimated and the load torque could be applied again.

The experimental results were also compared to the corresponding simulations carried out using accurate motor parameter estimates. Generally, the simulation results correspond very well to the experimental results — naturally, the simulated waveforms are smoother due to the absence of noise and parameter errors. The only significant difference was noticed between the experimental results shown in Fig. 7(a) and the corresponding simulation. When $\gamma_p = 10$ (Nm·s)$^{-1}$ corresponding to the experiment was used, the simulated system

[3]Since the PM servo motor acting as the loading machine cannot stand speeds much higher than 2 p.u., it was replaced with equal inertial mass in this experiment.

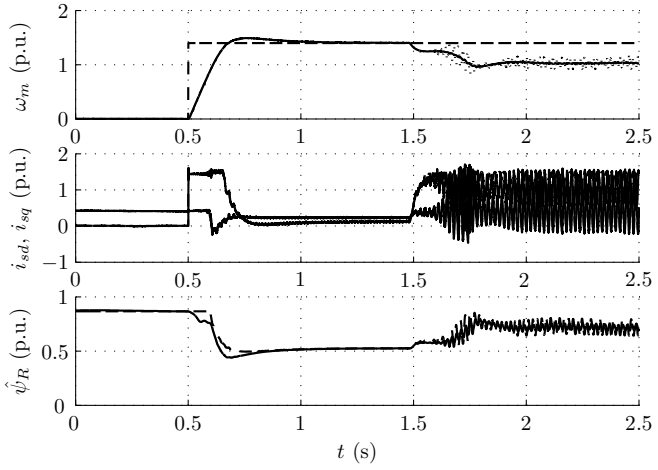

(a)

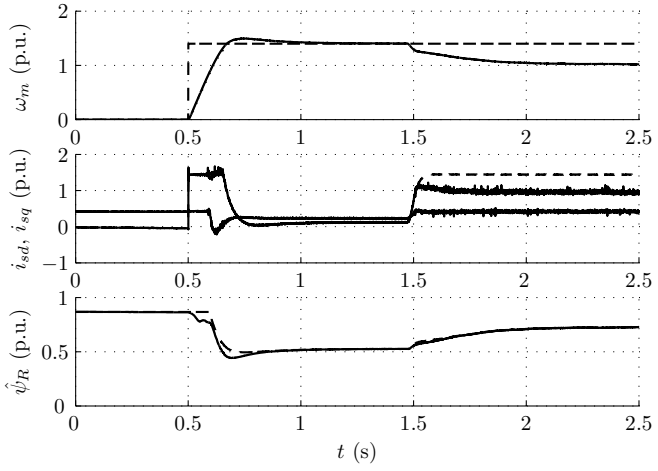

(b)

Fig. 7. Experimental results showing (a) instability phenomenon [corresponding to pole plot in Fig. 2(a)], and (b) its remedy by using proposed gains [corresponding to pole plot in Fig. 4(a)]. First subplot shows measured speed (solid), estimated speed (dotted), and speed reference (dashed). Second subplot shows d and q components of stator current (solid) and their references (dashed) in estimated flux reference frame. Third subplot presents magnitude of estimated rotor flux (solid) and its reference (dashed).

was stable. The instability became apparent when $\gamma_p < 6$ (Nm·s)$^{-1}$, which matches with the linearized model even better than the experimental results.

VIII. Conclusions

The linearized model of the observer is a useful tool when selecting the observer gain and the speed-adaptation gains of the speed-adaptive full-order flux observer. The linearized model reveals potential instability problems that are difficult to find by other means. A simple observer gain and a method to vary the speed-adaptation gains in the field-weakening region were proposed. Experimental results show stable operation in a very wide speed range.

Appendix A
Transformation of Observer Gains

Conventionally, the stator current and the rotor flux are used as state variables in full-order flux observers [1], [2], leading

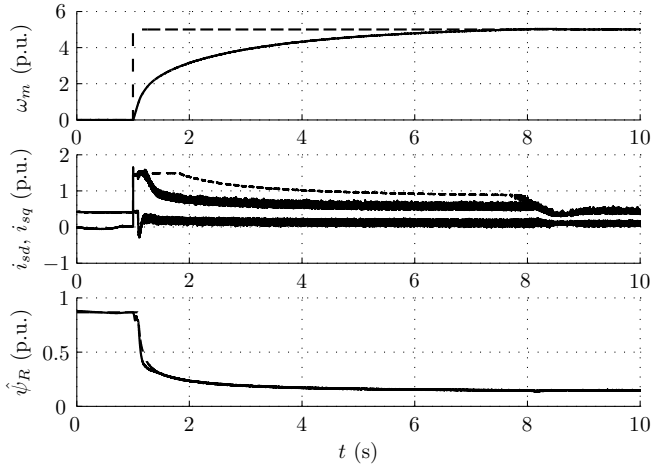

Fig. 8. Experimental results showing high-speed operation. Proposed gains were used. Explanations of curves are as in Fig. 7.

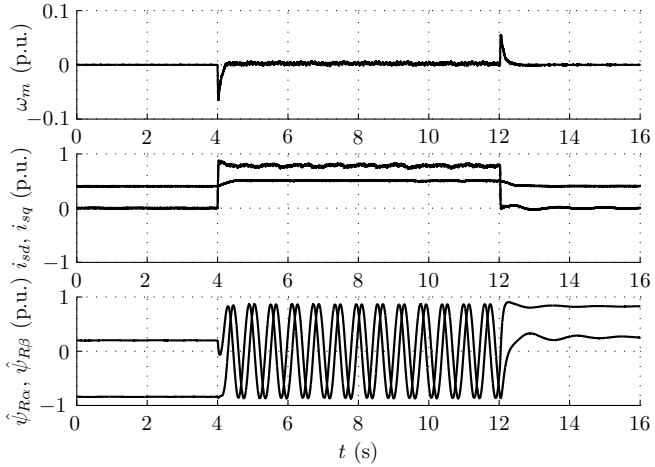

Fig. 9. Experimental results showing zero-speed operation when rated-load torque step is applied. Proposed gains were used. First subplot shows measured speed (solid) and estimated speed (dotted). Second subplot shows d and q components of stator current (solid) and their references (dashed) in estimated flux reference frame. Third subplot presents real and imaginary components of estimated rotor flux in stator reference frame.

to

$$\dot{\underline{\hat{\mathbf{z}}}} = \underline{\hat{\mathbf{F}}}\,\underline{\hat{\mathbf{z}}} + \mathbf{G}\underline{u}_s + \underline{\mathbf{K}}\big(\underline{i}_s - \underline{\hat{i}}_s\big) \tag{17a}$$

$$\underline{\hat{i}}_s = \mathbf{H}\underline{\hat{\mathbf{z}}} \tag{17b}$$

where the observer state vector is $\underline{\hat{\mathbf{z}}} = [\underline{\hat{i}}_s \quad \underline{\hat{\psi}}_R]^T$, the observer gain is $\underline{\mathbf{K}} = [\underline{k}_s \quad \underline{k}_r]^T$, and $\mathbf{H} = [1 \quad 0]$. The matrices $\underline{\hat{\mathbf{F}}}$ and $\mathbf{G}$ are given by

$$\underline{\hat{\mathbf{F}}} = \begin{bmatrix} -\frac{1}{\tau'_\sigma} - j\omega_k & \frac{1}{L'_s}\left(\frac{1}{\tau_r} - j\hat{\omega}_m\right) \\ R_R & -\frac{1}{\tau_r} - j\left(\omega_k - \hat{\omega}_m\right) \end{bmatrix}, \quad \mathbf{G} = \begin{bmatrix} \frac{1}{L'_s} \\ 0 \end{bmatrix} \tag{17c}$$

where $\tau_r = L_M/R_R$ and $\tau'_\sigma = L'_s/(R_s + R_R)$. It can be easily shown that the transformation

$$\underline{\mathbf{K}} = \begin{bmatrix} \frac{1}{L'_s} & -\frac{1}{L'_s} \\ 0 & 1 \end{bmatrix} \underline{\mathbf{L}} \tag{18}$$

gives identical behavior to observers (3) and (17).

Appendix B
Linearization

The linearized model (8) is straightforwardly obtained from (7) by considering the stator frequency ω_s as an input. However, it is more natural to consider ω_s as a function of the estimated rotor flux due to the coordinate transformations [13]. In the following, this linearization procedure is briefly described.

The estimated rotor flux reference frame is chosen, i.e., $\underline{\hat{\psi}}_R = \hat{\psi}_R + j0$ and $\omega_k = \omega_s$. The state-space representation (1) of the motor is divided into real and imaginary components

$$\dot{\psi}_{sd} = -\tfrac{1}{\tau'_s}\psi_{sd} + \omega_s\psi_{sq} + \tfrac{1}{\tau'_s}\psi_{Rd} + u_{sd} \tag{19a}$$

$$\dot{\psi}_{sq} = -\omega_s\psi_{sd} - \tfrac{1}{\tau'_s}\psi_{sq} + \tfrac{1}{\tau'_s}\psi_{Rq} + u_{sq} \tag{19b}$$

$$\dot{\psi}_{Rd} = \tfrac{1-\sigma}{\tau'_r}\psi_{sd} - \tfrac{1}{\tau'_r}\psi_{Rd} + (\omega_s - \omega_m)\,\psi_{Rq} \tag{19c}$$

$$\dot{\psi}_{Rq} = \tfrac{1-\sigma}{\tau'_r}\psi_{sq} - (\omega_s - \omega_m)\,\psi_{Rd} - \tfrac{1}{\tau'_r}\psi_{Rq} \tag{19d}$$

The observer (3) divided into components in the selected reference frame becomes

$$\begin{aligned}\dot{\hat{\psi}}_{sd} = {} & -\tfrac{1}{\tau'_s}\hat{\psi}_{sd} + \omega_s\hat{\psi}_{sq} + \tfrac{1}{\tau'_s}\hat{\psi}_R + u_{sd} \\ & + l_{sd}\big(i_{sd} - \hat{i}_{sd}\big) - l_{sq}\big(i_{sq} - \hat{i}_{sq}\big)\end{aligned} \tag{20a}$$

$$\begin{aligned}\dot{\hat{\psi}}_{sq} = {} & -\omega_s\hat{\psi}_{sd} - \tfrac{1}{\tau'_s}\hat{\psi}_{sq} + u_{sq} \\ & + l_{sd}\big(i_{sq} - \hat{i}_{sq}\big) + l_{sq}\big(i_{sd} - \hat{i}_{sd}\big)\end{aligned} \tag{20b}$$

$$\begin{aligned}\dot{\hat{\psi}}_R = {} & \tfrac{1-\sigma}{\tau'_r}\hat{\psi}_{sd} - \tfrac{1}{\tau'_r}\hat{\psi}_R \\ & + l_{rd}\big(i_{sd} - \hat{i}_{sd}\big) - l_{rq}\big(i_{sq} - \hat{i}_{sq}\big)\end{aligned} \tag{20c}$$

where

$$i_{sd} = \frac{\psi_{sd} - \psi_{Rd}}{L'_s}, \quad i_{sq} = \frac{\psi_{sq} - \psi_{Rq}}{L'_s} \tag{20d}$$

$$\hat{i}_{sd} = \frac{\hat{\psi}_{sd} - \hat{\psi}_R}{L'_s}, \quad \hat{i}_{sq} = \frac{\hat{\psi}_{sq}}{L'_s} \tag{20e}$$

and the stator frequency is solved from (3) by using the fact that the imaginary component of $\underline{\hat{\psi}}_R$ is zero:

$$\omega_s = \hat{\omega}_m + \frac{\tfrac{1-\sigma}{\tau'_r}\hat{\psi}_{sq} + l_{rd}\big(i_{sq} - \hat{i}_{sq}\big) + l_{rq}\big(i_{sd} - \hat{i}_{sd}\big)}{\hat{\psi}_R} \tag{21}$$

The stator frequency is eliminated from the state equations by inserting (21) into (19) and (20). The resulting system having inputs u_{sd}, u_{sq}, ω_m, and $\hat{\omega}_m$ is linearized. By introducing the new states, i.e., $e_{1d} = \psi_{sd} - \hat{\psi}_{sd}$, $e_{1q} = \psi_{sq} - \hat{\psi}_{sq}$, $e_{2d} = \psi_{Rd} - \hat{\psi}_R$, $e_{2q} = \psi_{Rq}$, combining the real and imaginary components, and using the matrix notation $\underline{\mathbf{e}} = \underline{\mathbf{x}} - \underline{\hat{\mathbf{x}}} = [\underline{e}_1 \quad \underline{e}_2]^T$, the linearized model (8) is obtained.

Acknowledgment

This work was financed in part by ABB Oy. The author gratefully acknowledges the contribution of Prof. J. Luomi. The author would also like to thank the reviewers for their professional work and helpful suggestions.

REFERENCES

[1] H. Kubota, K. Matsuse, and T. Nakano, "DSP-based speed adaptive flux observer of induction motor," *IEEE Trans. Ind. Applicat.*, vol. 29, no. 2, pp. 344–348, Mar./Apr. 1993.

[2] G. Yang and T.-H. Chin, "Adaptive-speed identification scheme for a vector-controlled speed sensorless inverter-induction motor drive," *IEEE Trans. Ind. Applicat.*, vol. 29, no. 4, pp. 820–825, July/Aug. 1993.

[3] H. Hofmann and S. R. Sanders, "Speed-sensorless vector torque control of induction machines using a two-time-scale approach," *IEEE Trans. Ind. Applicat.*, vol. 34, no. 1, pp. 169–177, Jan./Feb. 1998.

[4] G. Guidi and H. Umida, "A novel stator resistance estimation method for speed-sensorless induction motor drives," *IEEE Trans. Ind. Applicat.*, vol. 36, no. 6, pp. 1619–1627, Nov./Dec. 2000.

[5] H. Tajima, G. Guidi, and H. Umida, "Consideration about problems and solutions of speed estimation method and parameter tuning for speed-sensorless vector control of induction motor drives," *IEEE Trans. Ind. Applicat.*, vol. 38, no. 5, pp. 1282–1289, Sept./Oct. 2002.

[6] L. Harnefors and H.-P. Nee, "Full-order observers for flux and parameter estimation of induction motors," in *Proc. EPE'97*, vol. 3, Trondheim, Norway, Sept. 1997, pp. 375–381.

[7] J. Maes and J. A. Melkebeek, "Speed-sensorless direct torque control of induction motors using an adaptive flux observer," *IEEE Trans. Ind. Applicat.*, vol. 36, no. 3, pp. 778–785, May/June 2000.

[8] S. Suwankawin and S. Sangwongwanich, "A speed-sensorless IM drive with decoupling control and stability analysis of speed estimation," *IEEE Trans. Ind. Electron.*, vol. 49, no. 2, pp. 444–455, Apr. 2002.

[9] H. Kubota, I. Sato, Y. Tamura, K. Matsuse, H. Ohta, and Y. Hori, "Regenerating-mode low-speed operation of sensorless induction motor drive with adaptive observer," *IEEE Trans. Ind. Applicat.*, vol. 38, no. 4, pp. 1081–1086, 2002.

[10] M. Hinkkanen and J. Luomi, "Stabilization of regenerating mode operation in sensorless induction motor drives by full-order flux observer design," *IEEE Trans. Ind. Electron.*, vol. 51, no. 6, pp. 1318–1328, Dec. 2004.

[11] L. Harnefors, "Instability phenomena and remedies in sensorless indirect field oriented control," *IEEE Trans. Power Electron.*, vol. 15, no. 4, pp. 733–743, July 2000.

[12] B. Peterson, "Induction machine speed estimation – observations on observers," Ph.D. dissertation, Dept. Ind. Elect. Eng. Automat., Lund Univ., Lund, Sweden, Feb. 1996.

[13] L. Harnefors, "Design and analysis of general rotor-flux-oriented vector control systems," *IEEE Trans. Ind. Electron.*, vol. 48, no. 2, pp. 383–390, Apr. 2001.

[14] G. R. Slemon, "Modelling of induction machines for electric drives," *IEEE Trans. Ind. Applicat.*, vol. 25, no. 6, pp. 1126–1131, Nov./Dec. 1989.

[15] C. Schauder, "Adaptive speed identification for vector control of induction motors without rotational transducers," *IEEE Trans. Ind. Applicat.*, vol. 28, no. 5, pp. 1054–1061, Sept./Oct. 1992.

[16] M. Hinkkanen and J. Luomi, "Digital implementation of full-order flux observers for induction motors," in *Proc. EPE-PEMC'02*, Cavtat and Dubrovnik, Croatia, Sept. 2002, CD-ROM.

[17] M. Hinkkanen and J. Luomi, "Parameter sensitivity of full-order flux observers for induction motors," *IEEE Trans. Ind. Applicat.*, vol. 39, no. 4, pp. 1127–1135, July/Aug. 2003.

[18] F. Briz, M. W. Degner, and R. D. Lorenz, "Analysis and design of current regulators using complex vectors," *IEEE Trans. Ind. Applicat.*, vol. 36, no. 3, pp. 817–825, May/June 2000.

[19] F. Briz, A. Diez, M. W. Degner, and R. D. Lorenz, "Current and flux regulation in field-weakening operation [of induction motors]," *IEEE Trans. Ind. Applicat.*, vol. 37, no. 1, pp. 42–50, Jan./Feb. 2001.

[20] J. K. Pedersen, F. Blaabjerg, J. W. Jensen, and P. Thogersen, "An ideal PWM-VSI inverter with feedforward and feedback compensation," in *Proc. EPE'93*, vol. 4, Brighton, U.K., Sept. 1993, pp. 312–318.

Marko Hinkkanen was born in Rautjärvi, Finland, in 1975. He received the M.Sc. degree in electrical engineering in 2000 from Helsinki University of Technology, Espoo, Finland, where he is currently working toward the D.Sc. degree.

Since 2000, he has been with the Power Electronics Laboratory, Helsinki University of Technology, as a research scientist. His main research interest is the control of electrical drives.